scientific reports

OPEN

PTIP epigenetically regulates DNA damage-induced cell cycle arrest by upregulating PRDM1

Yuichiro Nakata[1,7✉], Shion Nagasawa[1,7], Yasuyuki Sera[2], Norimasa Yamasaki[3], Akinori Kanai[4], Kohei Kobatake[5], Takeshi Ueda[6], Miho Koizumi[2], Ichiro Manabe[1], Osamu Kaminuma[3] & Hiroaki Honda[2✉]

The genome is constantly exposed to DNA damage from endogenous and exogenous sources. Fine modulation of DNA repair, chromatin remodeling, and transcription factors is necessary for protecting genome integrity, but the precise mechanisms are still largely unclear. We found that after ionizing radiation (IR), global trimethylation of histone H3 at lysine 4 (H3K4me3) was decreased at an early (5 min) post-IR phase but increased at an intermediate (180 min) post-IR phase in both human and mouse hematopoietic cells. We demonstrated that PTIP, a component of the MLL histone methyltransferase complex, is required for H3K4me3 upregulation in the intermediate post-IR phase and promotes cell cycle arrest by epigenetically inducing a cell cycle inhibitor, PRDM1. In addition, we found that *PTIP* expression is specifically downregulated in acute myeloid leukemia patients. These findings collectively suggest that the PTIP-PRDM1 axis plays an essential role in proper DNA damage response and its deregulation contributes to leukemogenesis.

Keywords Histone methylation, PTIP, H3K4me3, DNA damage response

Cells have evolved highly orchestrated signaling pathways to repair DNA damage, since accumulation of DNA damage increases the risk of cancer[1]. In the DNA damage response (DDR), cells recognize lesions and transiently arrest cell cycle progression to allow time for repair[2]. DDR leads to cell cycle arrest, DNA repair, as well as apoptosis[3] and prolonged cell cycle arrest following DNA damage is essential for effective DNA repair[4]. DNA double-strand breaks (DSBs) are the most cytotoxic type of DNA damage that occurs following DNA replication, exposure to ionizing radiation (IR), and treatment with chemotherapeutic drugs[5]. DSBs are repaired by either non-homologous end joining (NHEJ) or homologous recombination (HR)[6]. 53BP1 plays central roles in the NHEJ pathway—it is recruited to DSBs, protects DNA ends from excessive resection, and promotes end-joining of DNA ends[7].

PTIP (PAX transcription activation domain interacting protein, also known as PAXIP1) contains multiple BRCA1 C-terminus (BRCT) domains that can interact with transcription factors and it functions as an adaptor protein downstream of p53-binding protein 1 (53BP1)[8,9]. PTIP is recruited by phosphorylated 53BP1 to promote the NHEJ pathway and PTIP-deficient cells are sensitive to DNA damage, indicating that PTIP is directly involved in DNA repair via formation of the 53BP1 complex[8,10–12]. On the other hand, PTIP functions as a component of the mixed-lineage leukemia (MLL) histone methyltransferase complexes that catalyze trimethylated histone H3 at lysine 4 (H3K4me3), a mark associated with gene activation[13,14]. Indeed, PTIP is required for transcriptional activation via epigenetic regulation, such as peroxisome proliferator-activated receptor gamma (PPARγ) activation in preadipocytes and osteoclasts[15] and sphingosine-1-phosphate receptor 1 (S1PR1) in T lymphocyte

[1]Department of Systems Medicine, Graduate School of Medicine, Chiba University, 1-8-1 Inohana, Chuo-Ku, Chiba-Shi, Chiba 260-8670, Japan. [2]Field of Human Disease Models, Major in Advanced Life Sciences and Medicine,, Institute of Laboratory Animals, Tokyo Women's Medical University, 8-1 Kawada-Cho, Shinjuku-Ku, Tokyo 162-8666, Japan. [3]Department of Disease Models, Research Institute for Radiation Biology and Medicine, Hiroshima University, 1-2-3 Kasumi, Minami-Ku, Hiroshima 734-8553, Japan. [4]Laboratory of Systems Genomics, Department of Computational Biology and Medical Sciences, Graduate School of Frontier Sciences, The University of Tokyo, 5-1-5 Kashiwanoha, Kashiwa, Chiba 277-8561, Japan. [5]Department of Urology, Institute of Biomedical and Health Sciences, Hiroshima University, 1-2-3 Kasumi, Minami-Ku, Hiroshima 734-8553, Japan. [6]Department of Biochemistry, Faculty of Medicine, Kindai University, 377-2 Ohnohigashi, Osakasayama-Shi, Osaka 589-8511, Japan. [7]These authors contributed equally: Yuichiro Nakata and Shion Nagasawa. ✉email: nakatay@chiba-u.jp; honda.hiroaki@twmu.ac.jp

egress[16]. Moreover, PTIP is associated with *Igh* germline transcription in B cell class switch recombination (CSR) by regulating H3K4me3 and promotes CSR[17–19]. Therefore, it is strongly suggested that PTIP contributes to cellular homeostasis through different functional properties.

Studies reported that methylation of histones at certain sites is associated with accessibility and recruitment of repair factors. Indeed, H3K4me3 and methylated H3K36 were found to promote the DDR pathway by recruiting repair factors[20–22]. In addition, H3K27me3, a gene repression mark, also promotes the NHEJ pathway through interaction with FANCD2, a key player in the DDR pathway[23]. While methylated histone marks induce alteration of chromatin structure and recruit repair factors to the lesion, transcriptional regulation by histone modifiers is also essential for DNA repair. For instance, EZH2, the histone methyltransferase catalyzing H3K27me3, promotes DNA repair by DNA damage-induced transcriptional silencing during the early phase following DNA damage[24]. In addition, H3K4me3 levels are upregulated to activate DDR genes at the intermediate phase of DNA damage[25].

Whether PTIP contributes to DDR not only as a component of the 53BP1 complex but also as an epigenetic factor regulating H3K4me3 levels is not known. Since a variety of mutations in DDR genes are associated with increased risk of developing leukemia[26], we explored whether PTIP-mediated H3K4me3 regulation has essential roles in DDR using human leukemia cell lines and mouse hematopoietic stem-progenitor cells (HSPCs). In this study, we provide evidence that at the intermediate post-IR phase, PTIP-mediated upregulation of H3K4me3 and subsequent induction of PRDM1 (also known as BLIMP1) are necessary for DDR mediated cell cycle arrest.

Results

DNA damage by IR induced alteration of global H3K4me3 levels

To examine whether H3K4me3 levels are altered following IR, we first performed fluorescent immunostaining and western blotting of phosphorylated H2AX (γH2AX), a marker of DNA damage, in human myeloid leukemia cell lines. In all three cell lines (HL-60, MOLM13, and K562), global H3K4me3 levels were significantly downregulated 5 min after IR but were significantly upregulated 180 min after IR in line with γH2AX accumulation, compared with 0 min (Fig. 1A–C and Supplementary Fig. 1A). Upregulated H3K4me3 levels gradually returned to baseline in a time-dependent manner (Supplementary Fig. 1B). To determine whether these observations were physiologically relevant, we performed the same experiment using primary mouse HSPCs (LSK cells; lineage [Mac-1, Gr-1, B220, Ter119, CD4 and CD8]⁻, c-kit⁺ and Sca-1⁺). Similar results were obtained at both time points (Fig. 1D), indicating that global H3K4me3 levels were downregulated in the early phase (5 min) following IR, likely due to DNA damage induced transcriptional silencing[27], but upregulated in the intermediate phase (180 min) following IR (hereafter, referred to as early post-IR and intermediate post-IR, respectively, two timepoints in DNA repair pathway activation) in normal and leukemic hematopoietic cells.

PTIP induces upregulation of global H3K4me3 levels at the intermediate phase after IR

Since PTIP mediates H3K4 methylation as part of a histone methyltransferase complex and the cell lines we tested do not possess mutations or deletions at the *PTIP* gene (COSMIC, https://cancer.sanger.ac.uk/cosmic), we examined whether PTIP contributes to the upregulation of H3K4me3 at intermediate post-IR. To this end, we produced *PTIP*-knockdown human leukemic cells and *Ptip* deficient mouse hematopoietic cells. For human cells, lentiviral-based control shRNA vector (*shCtrl*) and two independent shRNA vectors targeting *PTIP* (*shPTIP* #1 and #2) were transduced into HL-60 cells (Fig. 2A). In contrast to *shCtrl*-transduced HL-60 cells that exhibited significant upregulation of global H3K4me3 levels at 180 min after IR, no apparent changes were detected in *shPTIP*-transduced cells (Fig. 2B). The global H3K4me3 levels at 0 min after IR in *shCtrl, PTIP* (*shPTIP* #1 and #2)-transduced HL-60 cells were comparable, suggesting that PTIP deficiency may not affect H3K4me3 regulation at steady state (Fig. 2C). To obtain *Ptip*-deficient mouse hematopoietic cells, mice in which exon 7 was *floxed* (*Ptip^flox/flox*) were crossed with *ERT2Cre⁺* mice in which Cre was activated by tamoxifen, and *Ptip^flox/flox*, *ERT2Cre⁺* mice were treated with tamoxifen to generate *Ptip*-deficient (*Ptip^Δ/Δ*) mice (Fig. 2D). Tamoxifen-treated *Ptip^flox/flox*, *ERT2Cre⁻* mice were used as a *control* (*Ptip^+/+*). As observed in human leukemic cells, *Ptip^+/+* LSK cells exhibited marked upregulation of global H3K4me3 levels at 180 min after IR, which was observed to a lesser extent in *Ptip^Δ/Δ* cells (Fig. 2E). H3K4me3 upregulation in *Ptip^Δ/Δ* LSK cells was not completely diminished, potentially due to regulation of H3K4me3 by the COMPASS complex including SETD1A/B or by the COMPASS-like complex including MLL1/2. These results indicated that PTIP is required for upregulation of global H3K4me3 levels in both human and mouse hematopoietic cells at intermediate post-IR.

PTIP suppresses cell cycle progression after IR via upregulation of PRDM1

A previous report identified IR-responsive genes that are associated with DDR and upregulated after IR[25]. We thus hypothesized that PTIP contributes to DDR through a H3K4me3-mediated transcriptional program at intermediate post-IR. To investigate the expression changes of IR-responsive genes in leukemic cells, we first performed RT-qPCR using RNA extracted from HL-60 and MOLM13 cells before and after IR. We found that the expression of *PRDM1*, encoding a cell cycle inhibitor[28,29], was upregulated in both HL-60 and MOLM13 cells at 180 min after IR (Fig. 3A). Upregulation of *PRDM1* at 180 min after IR was markedly attenuated in *shPTIP*-transduced HL-60 cells compared with *shCtrl*-transduced cells (Fig. 3B). These findings strongly suggest that PTIP contributes to upregulation of *PRDM1* at intermediate post-IR. In addition, to explore the underlying transcriptional mechanisms, gene expression profiles of *shCtrl*- and *shPTIP* (#1 and #2)-transduced HL-60 cells at 0 min and 180 min after IR were examined by RNA-seq and the results were subjected to gene set enrichment analysis (GSEA) for pathway assessment (Fig. 3C and Supplementary Table. 1). In *shCtrl*-transduced HL-60 cells, gene sets associated with cell cycle proliferation (POSITIVE_REGULATION_OF_CELL_PROLIFERA-TION) were negatively enriched at 180 min after IR compared with 0 min, but no such effect was observed in *shPTIP*-transduced HL-60 cells (Fig. 3D, upper panels). Although no obvious changes were observed between
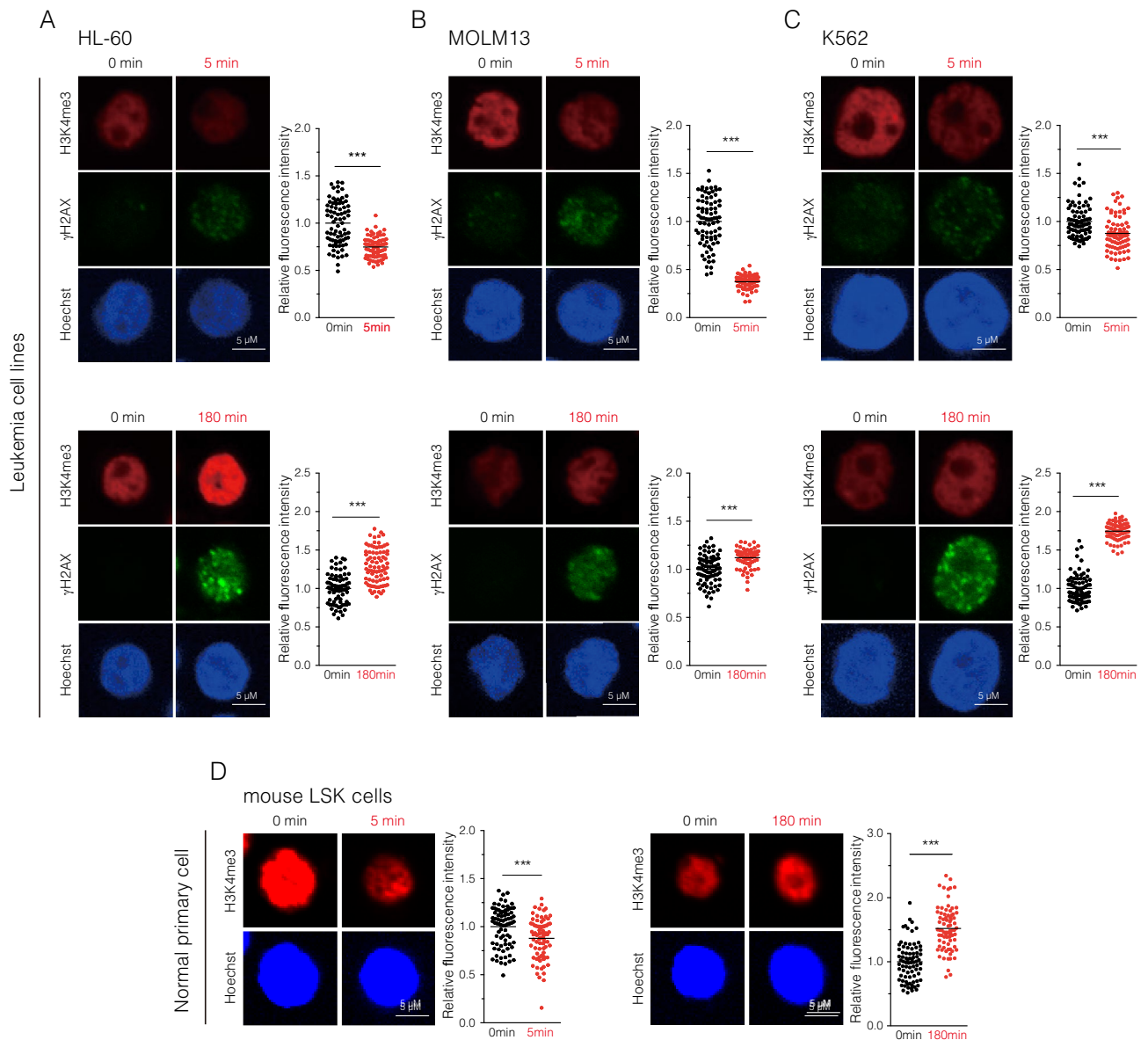
Figure 1. Alteration of H3K4me3 levels after IR in human leukemia cell lines and mouse hematopoietic stem/precursors cells (HSPCs). (**A-C**) Immunofluorescence staining (H3K4me3, γH2AX, and Hoechst) (left panels) and relative fluorescence intensity (H3K4me3) (right panels) in irradiated human leukemia cell lines: HL-60 (**A**), MOLM13 (**B**), and K562 (**C**). (**D**) Immunofluorescence staining (H3K4me3 and Hoechst) (left panels) and relative fluorescence intensity (H3K4me3) (right panels) in mouse LSK (lineage [Mac-1, Gr-1, B220, Ter119, CD4 and CD8]⁻, c-kit⁺ and Sca-1⁺) cells. The relative intensities at 5 min after ionizing radiation (IR) and 180 min after IR are compared with 0 min after IR. The mean values are indicated as bars (n = 80). ***$p < 0.001$.

shCtrl- and *shPTIP*-transduced HL-60 cells at 0 min after IR, these pathways were significantly positively enriched in *shPTIP*-transduced cells compared with *shCtrl*-transduced cells at 180 min after IR (Fig. 3D, lower panels). Following DNA damage, cell cycle checkpoints are activated and cell cycle arrest is transiently induced[2,7], suggesting that PTIP contributes to IR-induced cell cycle arrest.

To further investigate whether PTIP affects cell cycle activity via expression of *PRDM1*, we performed BrdU incorporation assays using IR-treated cells (Fig. 3E). We first examined the effect of IR on cell proliferation in HL-60 cells. As expected, IR-treated HL-60 cells exhibited markedly suppressed BrdU incorporation compared with untreated cells (Fig. 3F). We then performed the same assay using *shCtrl*- and *shPTIP*-transduced HL-60 cells. In contrast to *shCtrl*-transduced cells which exhibited significantly reduced BrdU incorporation, no such effects were detected in *shPTIP*-transduced cells (Fig. 3G). We further examined the effect of *PRDM1* knockdown on cell proliferation following IR. We confirmed downregulation of *PRDM1* with two different shRNAs (*shPRDM1* #1 and #2) (Fig. 3H) and found that IR-induced cell cycle inhibition was not detected in *shPRDM1*-transduced cells (Fig. 3I). These findings collectively indicate that the PTIP-PRDM1 axis is essential for IR-induced cell cycle arrest.
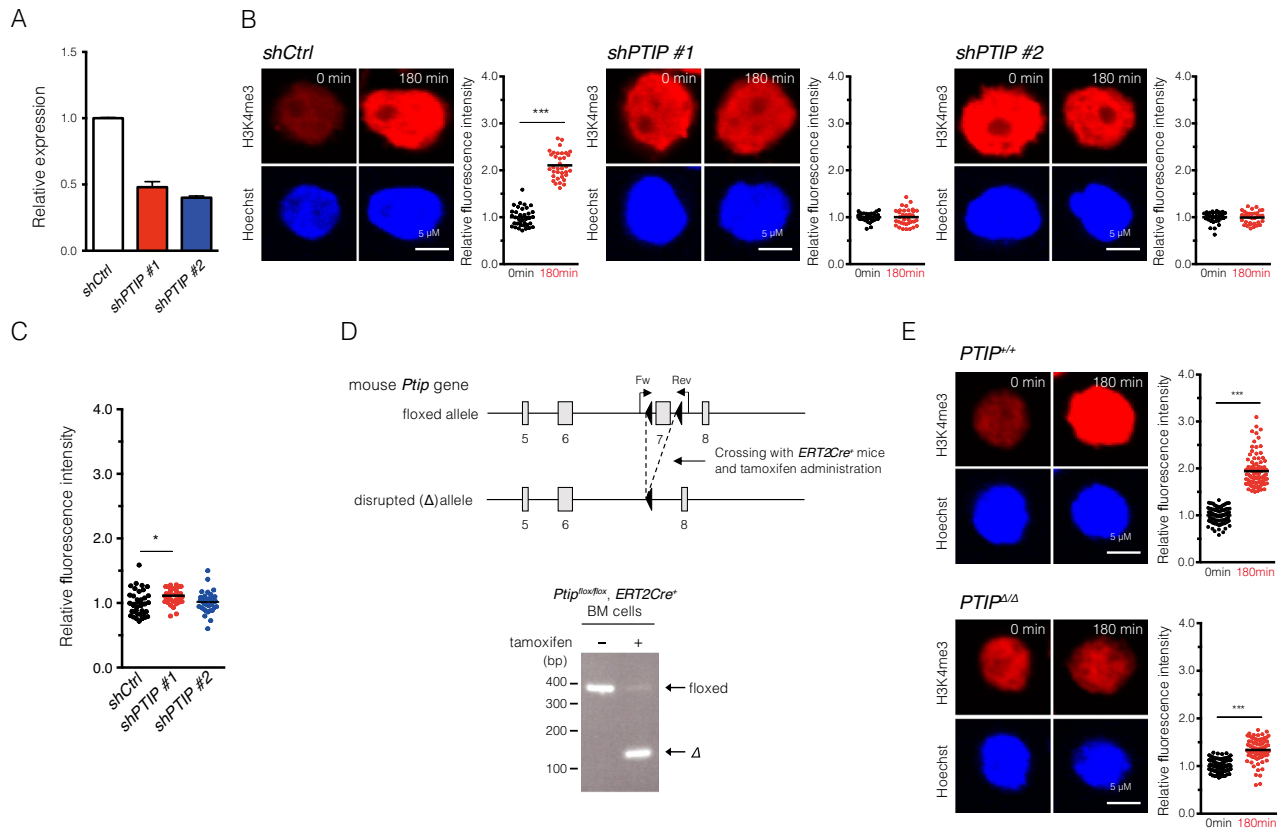
Figure 2. Alteration of H3K4me3 levels after IR in *PTIP*-deficient human leukemia cell lines and mouse HSPCs. (**A**) qPCR analysis of *PTIP* mRNA expression levels following introduction of *shCtrl* and *shPTIP* (#1 and #2) lentiviral vectors into HL-60 cells (mean + SD, n = 3). (**B**) Immunofluorescence staining (H3K4me3 and Hoechst) (left panels) and relative fluorescence intensity (H3K4me3) (right panels) in *shCtrl* (left), *shPTIP #1* (middle), and *shPTIP #2* (right) transduced HL-60 cells after IR. The relative intensity at 180 min after IR is compared with 0 min after IR for each cell line. The mean values are indicated as bars (n = 35). (**C**) H3K4me3 relative fluorescence intensity in *shCtrl* , *shPTIP #1*, and *shPTIP #2* transduced HL-60 cells at 0 min after IR. The relative intensity at 0 min after IR is compared with *shCtrl*. The mean values are indicated as bars (n = 35). (**D**) Generation of *Ptip*-deficient (*Ptip^{Δ/Δ}*) mice. Upper panel: mice in which exon 7 was *floxed* (*floxed* allele) were crossed with *ERT2Cre^+* mice in which Cre was activated by tamoxifen to generate *Ptip^{flox/flox}*, *ERT2Cre^+* mice, and exon 7 was deleted by tamoxifen administration (*disrupted (Δ)* allele). Lower panel: genomic PCR to detect *flox* allele-derived and *Δ* allele-derived products using bone marrow (BM) cells of tamoxifen-untreated (−) and -treated (+) *Ptip^{flox/flox}*, *ERT2Cre^+* mice. (**E**) Immunofluorescence staining (H3K4me3 and Hoechst) (left panels) and relative fluorescence intensity (H3K4me3) (right panels) of H3K4me3 in *Ptip^{+/+}* (upper) and *Ptip^{Δ/Δ}* (bottom) mouse LSK cells after IR. The relative intensity at 180 min after IR is compared with 0 min after IR in each group. The mean values are indicated as bars (n = 90). $*p < 0.05$, $***p < 0.001$.

A PTIP-containing MLL4 methyltransferase complex positively regulates H3K4me3 at the PRDM1 locus after IR

To explore the genome-wide distribution of H3K4me3, we performed CUT&RUN assays using HL-60 cells at 180 min after IR. In line with Fig. 1, genome-wide upregulation of H3K4me3 was observed in HL-60 cells after IR (Fig. 4A). We observed an increased number of H3K4me3 peaks (peak score > 3000, Supplementary Table. 2) at 180 min after IR compared with 0 min (Fig. 4B). In addition, the peaks were distributed genome-wide (Supplementary Fig. 2). The expression of H3K4me3 upregulated genes at 180 min after IR compared with 0 min, identified in Fig. 4B, was attenuated following PTIP knockdown (Fig. 4C). Motif analysis on these 1410 H3K4me3 peaks demonstrated greater enrichment for the E2F transcription factor, known to be associated with both cell cycle progression and cell cycle arrest[30]. Indeed, the putative target genes (± 3 kb from the transcription start sites (TSSs)) of these peaks are involved in the cell cycle pathway, which are different properties compared with the H3K4me3 peaks at 0 min (Fig. 4D,E and Supplementary Table. 3).

To explore the direct relationship between *PRDM1* expression and H3K4me3 upregulation, we analyzed whether H3K4me3 peaks accumulated at the *PRDM1* locus. As expected, enrichment of H3K4me3 at *PRDM1* was significantly increased downstream of the TSS in HL-60 cells at 180 min after IR compared with 0 min (Fig. 4F). In accordance with upregulation of H3K4me3, PTIP and MLL4 were also significantly enriched at this region at 180 min after IR compared with 0 min (Fig. 4G). In addition, H3K4me3 upregulation at 180 min after IR was attenuated by knockdown of PTIP (Fig. 4H). To investigate whether the regions downstream of the
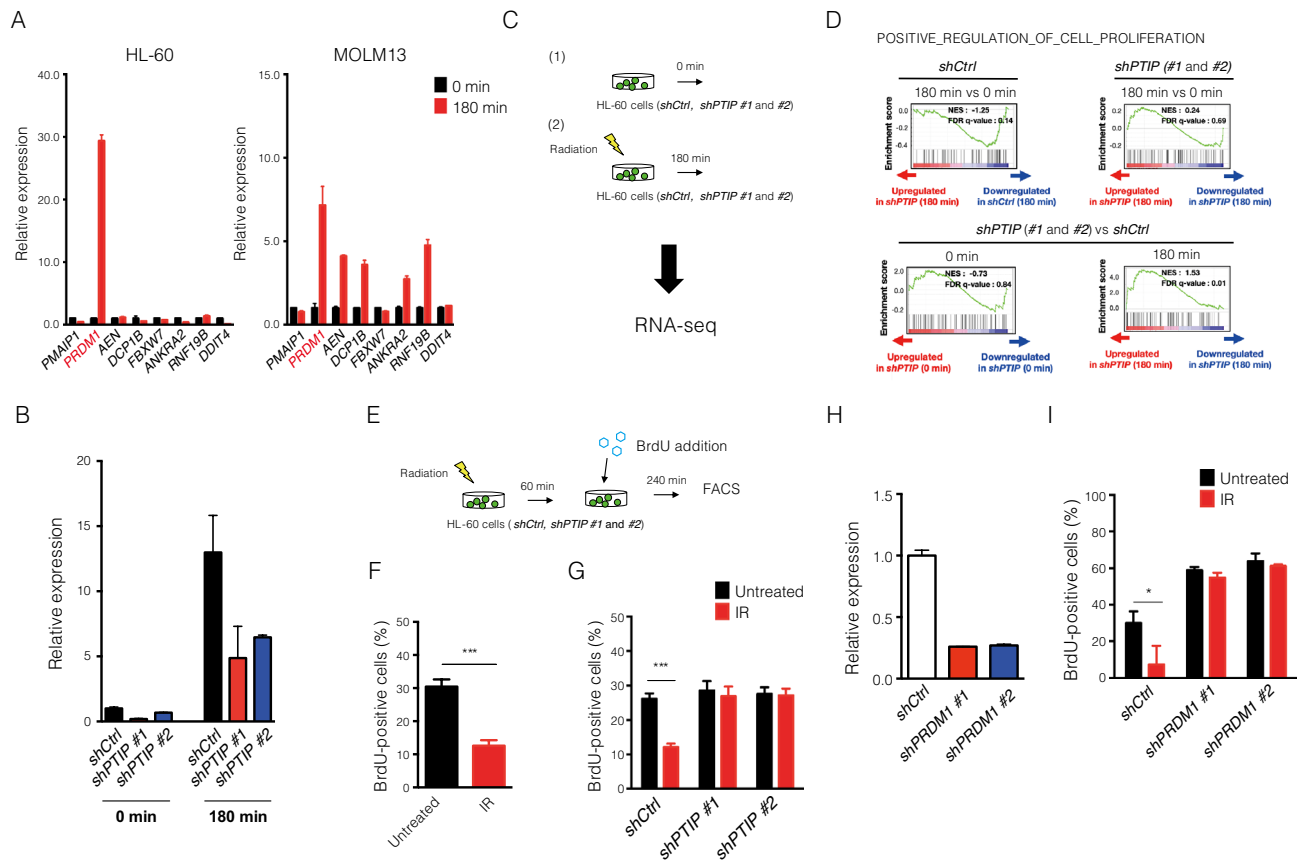
Figure 3. PTIP positively regulates *PRDM1* expression after IR to arrest the cell cycle. (**A**) qPCR analysis of mRNA expression levels of IR-induced genes[25] in HL-60 and MOLM13 cells. The expression each gene at 180 min after IR is compared with 0 min (mean + SD, n = 3). (**B**) qPCR analysis of *PRDM1* mRNA expression in HL-60 transfected with *shCtrl* and *shPTIP* (#1 and #2) at 0 min and at 180 min after IR. The relative expression levels are compared with *shCtrl* at 0 min after IR (mean + SD, n = 3). (**C**) Schematic illustration of RNA-seq in HL-60 transfected with *shCtrl* and *shPTIP* (#1 and #2) at 0 min and 180 min after IR. (**D**) GSEA plots associated with cell cycle progression (POSITIVE_REGULATION_OF_CELL_PROLIFERATION, from Human MSigDB Collections, C5: ontology gene sets) in HL-60 cells transduced with *shCtrl* and *shPTIP* (#1 and #2). HL-60 cells transfected with *shCtrl* at 180 min after IR relative to 0 min after IR and *shPTIP* at 180 min after IR relative to 0 min after IR are shown (upper panels). HL-60 cells transfected with *shPTIP* at 0 min after IR relative to *shCtrl* at 0 min and *shPTIP* (#1 and #2) at 180 min after IR relative to *shCtrl* at 180 min are shown (lower panels). (**E**) Schematic illustration of BrdU incorporation assays in HL-60 cells after IR. (**F**) Flow cytometric analysis of BrdU incorporation in untreated and IR-treated HL-60 cells (mean + SD, n = 3). (**G**) Flow cytometric analysis of BrdU incorporation in untreated and IR treated HL-60 cells transfected with *shCtrl* and *shPTIP* (#1 and #2) (mean + SD, n = 3). (**H**) qPCR analysis of *PRDM1* mRNA expression in HL-60 transfected with *shCtrl* and *shPRDM1* (#1 and #2) compared with *shCtrl* (mean + SD, n = 3). (**I**) Flow cytometric analysis of BrdU incorporation in untreated or irradiated HL-60 cells transfected with *shCtrl* and *shPRDM1* (#1 and #2) (mean + SD, n = 3). *NES* normalized enrichment score, *FDR* false discovery rate, *p < 0.05, ***p < 0.001.

PRDM1 TSS are essential for transcription, dCas9-VP64 with 4 types of guide RNA (gRNA): #1 upstream of TSS, #2 and #3 putative PRDM1 regulatory regions, and #4 downstream of exon 2, were recruited with lentiviral vectors (Fig. 4I). We found that #2 and #3 regions positively regulated transcription in accordance with increased H3K4me3 (Fig. 4J). Together, these findings demonstrate that an MLL4 methyltransferase complex containing PTIP directly upregulates H3K4me3 levels downstream of the *PRDM1* TSS, resulting in increased *PRDM1* expression and inhibited cell cycle progression in HL-60 cells at intermediate post-IR.

PTIP is downregulated in human AML

Given that PTIP is associated with DDR directly via DNA repair and with cell cycle regulation via histone modification, PTIP is assumed to function as a tumor suppressor. To assess the role of PTIP in leukemogenesis, we compared the expression of *PTIP* in human leukemic samples and cell lines. We found that *PTIP* mRNA expression was significantly downregulated in acute myeloid leukemia (AML) samples with different karyotypes and cell lines compared with normal stem/progenitor cells (Fig. 5A–C), strongly suggesting that PTIP may play a tumor suppressive role, possibly through activation of both DDR pathways.
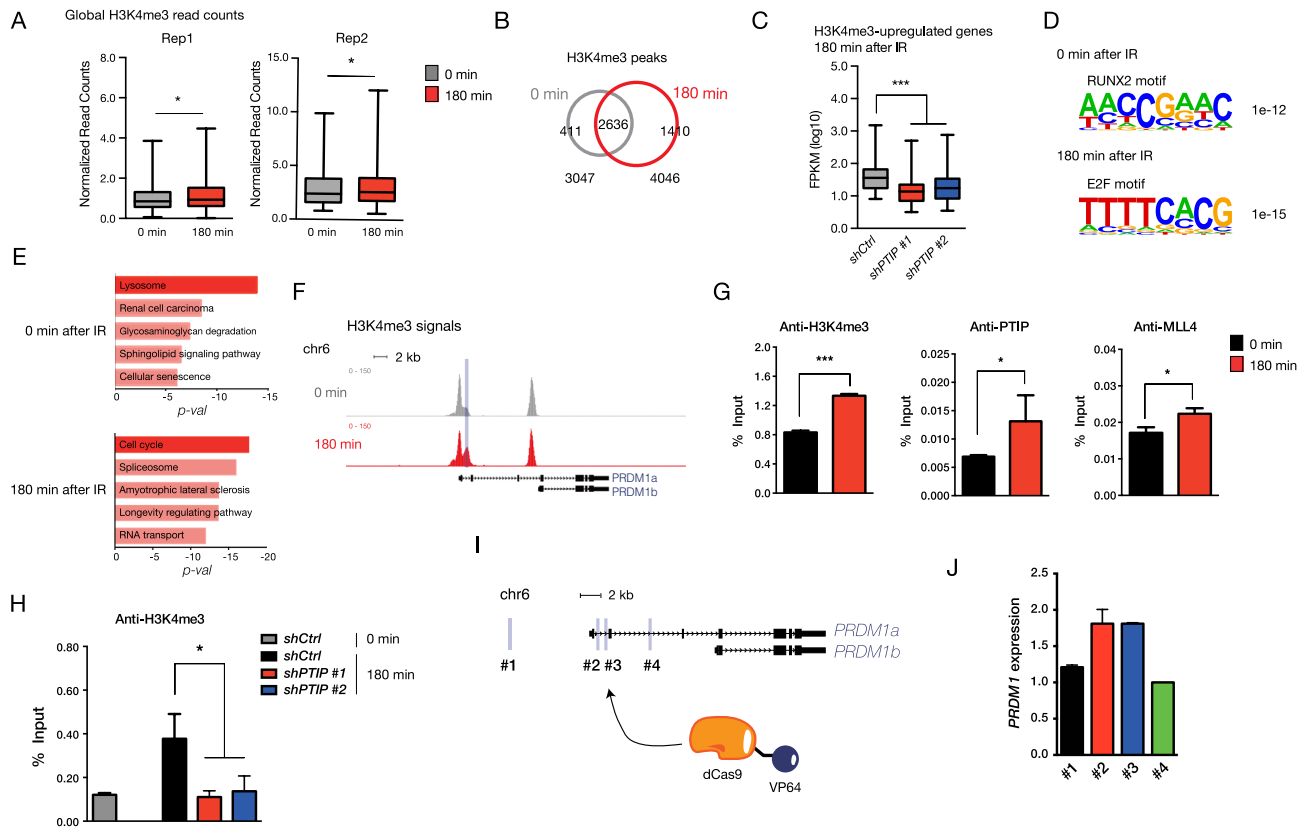
Figure 4. Epigenetic regulation of PTIP at the *PRDM1* locus. (**A**) Box plot showing global levels of H3K4me3 in HL-60 cells at 0 min and at 180 min after IR in two replicates (Rep1 and Rep2) normalized to each IgG sample. (**B**) Venn diagram showing H3K4me3 peaks (peak score > 3000) in HL-60 cells at 0 min and at 180 min after IR. (**C**) Expression of H3K4me3 upregulated genes in HL-60 cells transfected with *shCtrl* and *shPTIP* (*#1* and *#2*) at 180 min after IR. Genes were defined using peaks located ± 1 Kb from the TSS. (**D**) The top enriched transcription factor motifs from H3K4me3 peaks in HL-60 cells at 0 min after IR (top) at 180 min after IR (bottom). (**E**) Enrichr Pathway analysis (https://maayanlab.cloud/Enrichr/) enriched among putative target genes (± 3 kb from the TSS) from H3K4me3 peaks in HL-60 cells at 0 min after IR (top) at 180 min after IR (bottom). (**F**) Enrichment of H3K4me3 at the *PRDM1* locus in HL-60 cells at 0 min and at 180 min after IR in the UCSC genome browser. (**G**) ChIP-qPCR of H3K4me3 (left), PTIP (center) and MLL4 (right) at the *PRDM1* region in HL-60 cells at 0 min and 180 min after IR (mean + SD, n = 3). The primer product is indicated as blue box in Fig. 4F (**H**) ChIP-qPCR analysis of H3K4me3 in HL-60 cells transfected with *shCtrl* and *shPTIP* (*#1* and *#2*) at 0 min and at 180 min after IR. (**I**) Schematic illustration of the dCas9-VP64 system. gRNA positions are indicated as blue boxes (*#1* to *#4*). (**J**) qPCR of *PRDM1* mRNA in HL-60 cells expressing dCas9-VP64 transfected with *gRNA* (*#1* to *#4*). The relative expressions were compared with *gRNA #4* (mean + SD, n = 3). *$p < 0.05$, ***$p < 0.001$.

Discussion

It has been reported that trimethylation of H3K9 and H3K27, which changes the chromatin structure to a repressive state known as heterochromatin, plays essential roles for chromatin remodeling and transcriptional silencing in DDR[23,27,31]. On the other hand, H3K4me3 mediated by the MLL4 methyltransferase complex containing PTIP, changes chromatin structure to an active state, called euchromatin, and is also thought to be one of the critical histone modifications for DDR. However, the mechanism underlying H3K4me3 regulation associated with PTIP in DDR has remained controversial[20,21,25,32,33].

While several groups suggested the importance of H3K4me3 in DDR[25,33], others argued that the demethylation of H3K4me3 positively regulates DDR[20,21,32]. These contradictory results raise the question as to which mark (methylated or demethylated H3K4) is beneficial for DDR. In this study, we demonstrated that global H3K4me3 levels were downregulated at early (5 min) post-IR but upregulated at intermediate (180 min) post-IR in hematopoietic cells, which is in line with the results by Rashi-Elkeles, S. et al.[25] (Fig. 1). Our data support the idea that the contributions of H3K4me3 to DDR are time dependent. Indeed, treatment with JIB-04, an inhibitor of KDM5B, a demethylase of H3K4, in early post-IR induced an accumulation of H3K4me3 and impaired DNA repair pathways in non-small cell lung cancer (NSCLC) cells[21]. On the other hand, when NSCLC cells were treated with JIB-04 at intermediate post-IR, DNA repair pathway impairment was attenuated[23]. Additionally, highly compacted heterochromatin protects the genome from DNA damage but also suppresses repair efficiency and increases the mutation rate by creating a barrier to repair factor recruitment[33], indicating that chromatin
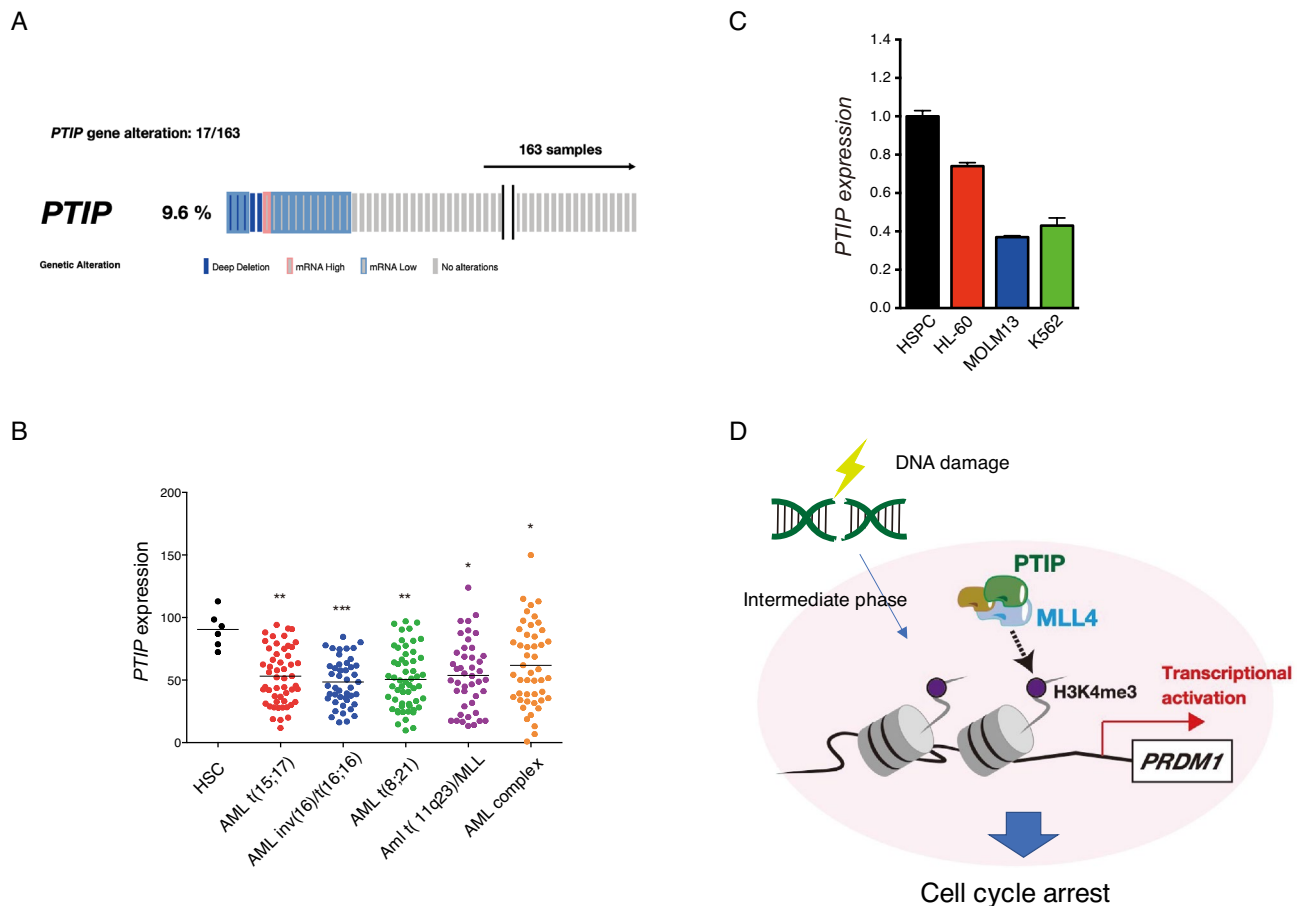
Figure 5. *PTIP* is downregulated in human acute myeloid leukemia (AML) and model. (**A**) *PTIP* alterations in human AML samples (n = 163) from the TCGA database (https://www.cbioportal.org). (**B**) Analysis of *PTIP* mRNA in AML cells with karyotypes of t(15;17), inv(16)/t(16;16), t(8;21), and t(11q23) translocations and the AML complex. The results of AML samples were compared with those of normal human hematopoietic stem cells (HSCs) using the Bloodspot database (https://www.fobinf.com, referred from BloodPool: AML samples vs. normal). The mean values are indicated as bars (n = 6–56). (**C**) qPCR analysis of *PRDM1* mRNA in leukemia cells (HL-60, MOLM and K562 cells). The relative expressions were compared with cord blood derived CD34$^+$ stem/progenitor cells as the normal cell control (mean + SD, n = 3) (**D**) Schematic illustration of PTIP-mediated regulation. At the intermediate phase after IR, an MLL4 complex containing PTIP upregulates global H3K4me3 levels. Expression of PRDM1, a cell cycle inhibitor, is activated by the complex via epigenetic regulation which induces cell cycle arrest to promote the DNA damage response. $*p < 0.05$, $**p < 0.01$ and $***p < 0.001$.

structure should be altered at the proper phase in DDR. These results imply that accumulation of H3K4me3 is dispensable or toxic for DDR at early post-IR but crucial for DDR at intermediate post-IR.

PTIP deficiency suppressed accumulation of H3K4me3 and promoted cell proliferation pathways at intermediate post-IR (Figs. 2, 3A), suggesting that PTIP possibly fine-tunes cell cycle progression at intermediate post-IR via H3K4me3 regulation. Our findings also highlighted that PTIP mediates expression of PRDM1, which functions as both a cell cycle inhibitor[8,29] and an IRinduced protein[25] by upregulating H3K4me3 in cooperation with MLL4 (Figs. 3, 4). Thus, PTIP is crucial for temporal cell cycle arrest after IR and for the DNA repair process.

In this study, we demonstrated that following DNA damage, downregulation of H3K4me3 was observed as a primary event and upregulation of H3K4me3 by an MLL4 methyltransferase complex containing PTIP occurred as a secondary event to induce cell cycle arrest via *PRDM1* activation (Fig. 5D). Understanding this mechanism may also shed light on the multifaceted functions of PTIP. In addition, to address the issue that PTIP functions as a tumor suppressive factor through activation of both DDR pathways in greater detail, future studies can aim to investigate whether $Ptip^{\Delta/\Delta}$ mice develop leukemia spontaneously via in vivo mutagenesis using retroviral transduction assays and exposure to a chemical carcinogen.

Materials and methods
Cells and mice
Human leukemia cell lines (HL-60, MOLM13, and K562), provided by Dr. Toshiya Inaba (Hiroshima University, Hiroshima, Japan), were grown in RPMI-1640 medium containing 10% fetal bovine serum supplemented with penicillin and streptomycin. The detailed procedures for construction of the targeting vector and generation of the cKI mice are described in Fig. 2C. *CreERT2* + mice (C57BL/6-Gt(ROSA)26Sortm1(cre/Est1)Arte) were

purchased from Taconic Biosciences (Hudson, NY, USA). Cre activation was achieved by intraperitoneal admin-istration tamoxifen (Sigma, T5648). The all animal experiments complied with the ARRIVE guidelines and were conducted in accordance with the Guide for the Care and Use of Laboratory Animals of Hiroshima University Animal Research Committee (permission no. A17-84). Cervical dislocation under light anesthesia was per-formed as a euthanasia method for mice according to the American Veterinary Medical Association (AVMA) Guidelines. Mouse HSPCs (LSK cells) were stained with antibodies listed in Supplementary Table. 4 and sorted with a FACSAria II (BD Biosciences). LSK cells were grown in S-clone SF-O3 serum-free medium (Iwai North America Inc.) containing 1% BSA supplemented with cytokines (100 ng/mL mouse SCF, 100 ng/mL mouse TPO, 100 ng/mL mouse FLT3L and 50 ng/mL mouse IL-6) (Pepro Tec). CB derived human $CD34^+$ stem/progenitor cells (Lonza) were cultured in StemSpan (Stem Cell Technologies) with 50 ng/mL human SCF (PeproTech), 50 ng/mL human TPO (PeproTech), and 50 ng/mL human Flt3-ligand (PeproTech). The cells were maintained in a humidified, 5% CO_2 atmosphere at 37 ℃. Cultured $CD34^+$ cells were stained with antibodies listed in Sup-plementary Table. 4 and sorted as described above.

Radiation treatment

Cells were irradiated with X-rays using a CP-160 (Acrobio). Total radiation dose was as follows: 5 Gy in human leukemia cell lines and 2 Gy in LSK cells from $Ptip^{+/+}$ and $Ptip^{\Delta/\Delta}$ mice. After IR, cells were incubated for the indicated time periods at 37 ℃.

Immunofluorescent staining

Cells were plated on poly-L-lysine-coated glass slides (Matsunami Glass), fixed with 4% paraformaldehyde, permeabilized with 0.5% Triton X-100 and treated with Protein block serum-free (Dako) to block non-specific binding. Subsequently, the cells were stained with anti-H3K4me3 and anti-γH2AX antibodies (Supplementary Table. 4). After washing with PBS, the cells were stained with Alexa Fluor 488- or 555-conjugated anti-rabbit and mouse IgG antibodies (Invitrogen). The nuclei were counterstained with Hoechst 33342 (Dojindo Laboratories). Images were taken with an FV-1000 confocal microscope (Olympus) and the fluorescence intensity of individual cells was computationally quantified using ImageJ64 software and were normalized against the mean fluorescence intensity of each control cell type (0 min after IR), as the relative fluorescence intensity[34].

Lentiviral vector transduction

To produce lentivirus containing supernatant, *pLV-H1-shRNA-EF1α-GFP-Bsd* (Biosettia), *EF1α-dCas9-VP64-EGFP*, *Lenti-gRNA-EF1α-BleoR* (kindly provided from Dr. Hoshii, Chiba university), *Gag-Pol*, *Rev*, and *VSV-G* expression vectors (Addgene) were transduced into Lenti-X 293 T cells (Takara Bio Inc.) with Lipofectamine 2000 (Invitrogen) and concentrated with Lenti-X concentrator (Takara Bio Inc.). In knockdown experiments, HL-60 cells were infected with lentivirus containing supernatant carrying *shCtrl*, *shPTIP* (#1 and #2) and *shPRDM1* (#1 and #2). The cell lines were established and expanded before radiation treatment. In dCas9 experiments, HL-60 cells were infected with lentiviral supernatant containing dCas9-VP64 and gRNA (*#1* to *#4*). The shRNA and gRNA sequences are listed in Supplementary Table. 5.

Quantitative real-time PCR

Total cellular RNA was isolated with TRIZOL reagent (Invitrogen) and reverse-transcribed with a SuperScript VILO master mix kit (Invitrogen) according to the manufacturer's protocol. Quantitative real-time PCR was performed with power SYBR Green PCR Master Mix (Thermo Fisher Scientific) on a StepOnePlus Real-Time PCR system (Applied Biosystems). The primer sequences are listed in Supplementary Table. 5. All data are presented relative to *GAPDH*.

Histone extraction and western blotting

Cells were resuspended in pH 6.5 lysis buffer (10 mM Tris- HCl at pH 8, 50 mM sodium bisulfite, 1% Triton X-100, 10 mM MgCl2, 8.6% sucrose, 10 mM sodium butyrate). After the supernatant was discarded, the pellet was washed with pH 7.4 wash buffer (10 mM Tris, 13 mM EDTA). After the supernatant was discarded, the pellet was dissolved in 0.4 M H_2SO_4 for 1 h on ice. The supernatant was collected into a new tube including 80% of acetone and incubated overnight at −20 ℃. After the supernatant was discarded, the pellets were air-dried and resuspended in water. Histone concentration was assayed using Bradford assay. Three micrograms of total histone extract were loaded into a 15% SDS-PAGE gel. Western blotting was performed as previously described[35].

RNA-seq and analysis

Total RNA from duplicate samples (*shPTIP* #1 and #2) was extracted with RNeasy mini kit (QIAGEN) and RNA-Seq libraries were prepared with the TruSeq Stranded mRNA Library Prep Kit (Illumina). Transcriptome analysis was performed using a next-generation sequencer (HiSeq 2500; Illumina) according to the manufac-turer's instructions. The generated sequence tags (more than 2.0×10^7 reads for each sample) were mapped onto the human genomic sequence (UCSC Genome Browser, version hg19) with the sequence alignment program Tophat. Transcriptomes were compared with FPKM values and analyzed with Gene Set Enrichment Analysis (GSEA_4.3.3) software (Broad Institute, https://www.gsea-msigdb.org/gsea/index.jsp). Gene sets with a false discovery rate (FDR) q-value of < 0.25 were considered statistically significant.

BrdU incorporation analysis

BrdU incorporation was analyzed with a BrdU Flow Kit (BD Biosciences). Pre-cultured HL-60 cells 60 min after IR were treated with BrdU (10 μM) into cultured medium 240 min before the analysis. Cells were fixed, permeabilized and stained with an anti-BrdU antibody conjugated APC (Supplementary Table. 4). BrdU positive cells were measured with a FACSCanto II (BD Biosciences). Data were analyzed with FlowJo v10.10 software (BD Biosciences).

ChIP-qPCR analysis

Chromatin was enzymatically shred and immunoprecipitated with the ChIP-IT Express Enzymatic Kit (Active Motif) according to the manufacturer's instructions. Antibodies are listed in Supplementary Table. 4. Subsequently, the chromatin was cleaned up with a QIAquick PCR purification kit (QIAGEN). Primer sequences are listed in Supplementary Table. 5.

CUT&RUN assay and analysis

Anti-H3K4me3 and anti-IgG antibodies, listed in Supplementary Table. 4, were used for CUT&RUN performed with the CUT&RUN assay kit (Cell Signaling), according to the manufacturer's protocol. Libraries were generated using the NEBNext Ultra II DNA Library Prep Kit for Illumina (NEB, E7370L) and sequenced on an Illumina NovaSeq 6000. Paired-end fastq files were processed using the ENCODE Transcription Factor and Histone ChIP-Seq pipeline (https://github.com/ENCODE-DCC/chip-seq-pipeline2). Reads were trimmed using cutadapt v2.5. Reads were aligned to the hg19 genome using Bowtie2 v2.3.4.3, and SAMtools v1.9 was used to convert the output file to BAM format. Duplicates were removed using Picard Tools v2.20.7. Peak calling was performed with MACS2 v2.2.4, and the peaks compared with each IgG sample for subsequent analysis. Narrow peaks (1142–10293 bp, peak score: > 3000) were detected as H3K4me3 enriched peaks, listed in Supplementary Table. 1. Bigwig files were normalized by a scaling factor using Deeptools v3.3.1and bamCoverage tools and visualized in the UCSC genome browser (https://genome.ucsc.edu). The scaling factors were calculated by determining the number of spike-in DNA reads and normalized to total sequencing depth. Homer v4.11 was used for peak annotation and motif analysis. Bedtools v2.29.0 intersect was used to determine overlapping peaks (with at least 1 bp overlap) and assign target genes.

Statistical analysis

The statistical significance of differences between two samples was assessed by two-tailed Student's t test. When multiple samples were compared, the statistical significance of differences was assessed using one-way ANOVA followed by Dunnett's test. All statistical tests were performed with Prism software version 6 (GraphPad). All data were obtained from at least two independent experimental replicates. In quantitative real-time PCR, SDs were calculated with technical triplicates, thus statistical significance was not shown.

Data availability

The datasets generated and analyzed during the current study are available in the DNA Data Bank of Japan (DDBJ) repository (https://www.ddbj.nig.ac.jp/) (RNA-seq; DRA010427 and CUT&RUN; DRA016981 (rep1) and DRA018596 (rep2)).

References

1. Groelly, F. J., Fawkes, M., Dagg, R. A., Blackford, A. N. & Tarsounas, M. Targeting DNA damage response pathways in cancer. *Nat. Rev. Cancer* **23**(2), 78–94 (2023).
2. Shaltiel, I. A., Krenning, L., Bruinsma, W. & Medema, R. H. The same, only different - DNA damage checkpoints and their reversal throughout the cell cycle. *J. Cell Sci.* **128**(4), 607–620 (2015).
3. Clay, D. E. & Fox, D. T. DNA damage responses during the cell cycle: Insights from model organisms and beyond. *Genes (Basel)* **12**(12), 1882 (2021).
4. Zhou, F. X. *et al.* Prolonged cell cycle arrest in response to DNA damage in yeast requires the maintenance of DNA damage signaling and the spindle assembly checkpoint. *eLife* https://doi.org/10.7554/eLife.94334.1 (2024).
5. Mehta, A. & Haber, J. E. Sources of DNA double-strand breaks and models of recombinational DNA repair. *Cold Spring Harb. Perspect. Biol.* **6**(9), a016428 (2014).
6. Ceccaldi, R., Rondinelli, B. & D'Andrea, A. D. Repair pathway choices and consequences at the double-strand break. *Trends Cell Biol.* **26**(1), 52–64 (2016).
7. Hustedt, N. & Durocher, D. The control of DNA repair by the cell cycle. *Nat. Cell Biol.* **19**(1), 1–9 (2016).
8. Wang, J. *et al.* PTIP associates with Artemis to dictate DNA repair pathway choice. *Genes Dev.* **28**(24), 2693–2698 (2014).
9. Wu, J., Prindle, M. J., Dressler, G. R. & Yu, X. PTIP regulates 53BP1 and SMC1 at the DNA damage sites. *J. Biol. Chem.* **284**(27), 18078–18084 (2009).
10. Jowsey, P. A., Doherty, A. J. & Rouse, J. Human PTIP facilitates ATM-mediated activation of p53 and promotes cellular resistance to ionizing radiation. *J. Biol. Chem.* **279**(53), 55562–55569 (2004).
11. Munoz, I. M., Jowsey, P. A., Toth, R. & Rouse, J. Phospho-epitope binding by the BRCT domains of hPTIP controls multiple aspects of the cellular response to DNA damage. *Nucleic Acids Res.* **35**(16), 5312–5322 (2007).
12. Callen, E. *et al.* 53BP1 mediates productive and mutagenic DNA repair through distinct phosphoprotein interactions. *Cell* **153**(6), 1266–1280 (2013).
13. Cho, Y. W. *et al.* PTIP associates with MLL3- and MLL4-containing histone H3 lysine 4 methyltransferase complex. *J. Biol. Chem.* **282**(28), 20395–20406 (2007).
14. Patel, S. R., Kim, D., Levitan, I. & Dressler, G. R. The BRCT-domain containing protein PTIP links PAX2 to a histone H3, lysine 4 methyltransferase complex. *Dev. Cell* **13**(4), 580–592 (2007).

15. Cho, Y. W. *et al.* Histone methylation regulator PTIP is required for PPARgamma and C/EBPalpha expression and adipogenesis. *Cell Metab.* **10**(1), 27–39 (2009).
16. Callen, E. *et al.* The DNA damage- and transcription-associated protein paxip1 controls thymocyte development and emigration. *Immunity* **37**(6), 971–985 (2012).
17. Daniel, J. A. *et al.* PTIP promotes chromatin changes critical for immunoglobulin class switch recombination. *Science* **329**(5994), 917–923 (2010).
18. Schwab, K. R., Patel, S. R. & Dressler, G. R. Role of PTIP in class switch recombination and long-range chromatin interactions at the immunoglobulin heavy chain locus. *Mol. Cell. Biol.* **31**(7), 1503–1511 (2011).
19. Starnes, L. M. *et al.* A PTIP-PA1 subcomplex promotes transcription for IgH class switching independently from the associated MLL3/MLL4 methyltransferase complex. *Genes Dev.* **30**(2), 149–163 (2016).
20. Li, X. *et al.* Histone demethylase KDM5B is a key regulator of genome stability. *Proc. Natl. Acad. Sci. U. S. A.* **111**(19), 7096–7101 (2014).
21. Bayo, J. *et al.* Jumonji inhibitors overcome radioresistance in cancer through changes in H3K4 methylation at double-strand breaks. *Cell Rep.* **25**(4), 1040-1050.e5 (2018).
22. Pai, C. C. *et al.* A histone H3K36 chromatin switch coordinates DNA double-strand break repair pathway choice. *Nat. Commun.* **5**, 4091 (2014).
23. Zhang, Y. *et al.* Histone H3K27 methylation modulates the dynamics of FANCD2 on chromatin to facilitate NHEJ and genome stability. *J. Cell Sci.* **131**(12), jcs215525 (2018).
24. Kakarougkas, A. *et al.* Requirement for PBAF in transcriptional repression and repair at DNA breaks in actively transcribed regions of chromatin. *Mol. Cell.* **55**(5), 723–732 (2014).
25. Rashi-Elkeles, S. *et al.* Parallel profiling of the transcriptome, cistrome, and epigenome in the cellular response to ionizing radiation. *Sci. Signal.* **7**(325), rs3 (2014).
26. Esposito, M. T. & So, C. W. DNA damage accumulation and repair defects in acute myeloid leukemia: Implications for pathogenesis, disease progression, and chemotherapy resistance. *Chromosoma* **123**(6), 545–561 (2014).
27. Capozzo, I., Iannelli, F., Francia, S. & d'Adda di Fagagna, F. Express or repress? The transcriptional dilemma of damaged chromatin. *FEBS J.* **284**(14), 2133–2147 (2017).
28. Wan, Z., Lu, Y., Rui, L., Yu, X. & Li, Z. PRDM1 overexpression induce G0/G1 arrest in DF-1 cell line. *Gene* **592**(1), 119–127 (2016).
29. Liu, C. *et al.* PRDM1 silences stem cell-related genes and inhibits proliferation of human colon tumor organoids. *Proc. Natl. Acad. Sci. U. S. A.* **115**(22), E5066–E5075 (2018).
30. Bracken, A. P., Ciro, M., Cocito, A. & Helin, K. E2F target genes: Unraveling the biology. *Trends Biochem. Sci.* **29**(8), 409–417 (2004).
31. Ayrapetov, M. K., Gursoy-Yuzugullu, O., Xu, C., Xu, Y. & Price, B. D. DNA double-strand breaks promote methylation of histone H3 on lysine 9 and transient formation of repressive chromatin. *Proc. Natl. Acad. Sci. U. S. A.* **111**(25), 9169–9174 (2014).
32. Gong, F., Clouaire, T., Aguirrebengoa, M., Legube, G. & Miller, K. M. Histone demethylase KDM5A regulates the ZMYND8-NuRD chromatin remodeler to promote DNA repair. *J. Cell Biol.* **216**(7), 1959–1974 (2017).
33. Fortuny, A. & Polo, S. E. The response to DNA damage in heterochromatin domains. *Chromosoma* **127**(3), 291–300 (2018).
34. Seita, J. *et al.* Lnk negatively regulates self-renewal of hematopoietic stem cells by modifying thrombopoietin-mediated signal transduction. *Proc. Natl. Acad. Sci. U. S. A.* **104**(7), 2349–2354 (2007).
35. Nakata, Y. *et al.* Acquired expression of Cbl^{Q367P} in mice induces dysplastic myelopoiesis mimicking chronic myelomonocytic leukemia. *Blood* **129**(15), 2148–2160 (2017).
36. Ikeda, K. *et al.* Maintenance of the functional integrity of mouse hematopoiesis by EED and promotion of leukemogenesis by EED haploinsufficiency. *Sci. Rep.* **6**, 29454 (2016).
37. Sera, Y. *et al.* UTX maintains the functional integrity of the murine hematopoietic system by globally regulating aging-associated genes. *Blood* **137**(7), 908–922 (2021).
38. Panchenko, T. *et al.* Histone H3.3 phosphorylation amplifies stimulation-induced transcription. *Nature* **583**(7818), 852–857 (2020).
39. Leiendecker, L. *et al.* LSD1 inhibition induces differentiation and cell death in Merkel cell carcinoma. *EMBO Mol. Med.* **12**(11), e12525 (2020).
40. Guo, P. *et al.* Histone variant H3.3 maintains adult haematopoietic stem cell homeostasis by enforcing chromatin adaptability. *Nat. Cell Biol.* **24**(1), 99–111 (2022).
41. Lee, J. E. *et al.* H3K4 mono- and di-methyltransferase MLL4 is required for enhancer activation during cell differentiation. *Elife* **2**, e01503 (2013).
42. Callen, E. *et al.* The DNA damage- and transcription-associated protein paxip1 controls thymocyte development and emigration. *Immunity* **37**(6), 971–985 (2012).

Author contributions

Y.N. and H.H. designed the study. H.H., N.Y., and M. K. constructed the targeting vectors and generated genetically engineered mice. Y.N. and A.K. performed RNA-seq analysis. Y.N. and K.K. performed immunofluorescent staining and flow cytometric analysis. Y.N., S.N., and Y.S. performed Cut &Run, ChIP-qPCR and dCas9 assays. Y.N., T.U., I.M., O.K., and H.H. wrote and revised the manuscript. All authors reviewed and agreed on the final version of the manuscript.

Funding

Competing interests

The authors declare no competing interests.

Additional information

Supplementary Information The online version contains supplementary material available at https://doi.org/10.1038/s41598-024-68295-w.

Correspondence and requests for materials should be addressed to Y.N. or H.H.

Reprints and permissions information is available at www.nature.com/reprints.

Publisher's note Springer Nature remains neutral with regard to jurisdictional claims in published maps and institutional affiliations.